Modular 2SB SIS Receiver for 600–720 GHz: Performance and Characterization Methods

Andrey Khudchenko, Ronald Hesper, Andrey M. Baryshev, Jan Barkhof, and Fausto Patricio Mena

***Abstract*—A modular sideband-separating (2SB) receiver for 600–720 GHz has been built and tested. The used modular design allows to characterize all the parts separately, including testing of the superconductor–insulator–superconductor (SIS) junctions individually in a double-sideband mode before building them in to the 2SB assembly. The developed 2SB mixer has a single sideband noise temperature below 380 K in the entire operating band and reaches a level of 200 K in the best point. At the same time, the image rejection ratio (IRR) was demonstrated to be better than 11.5 dB over the entire band. However, we have found a discrepancy between the observed and expected performance. To investigate this problem, we have developed and applied methods to characterize RF and intermediate frequency imbalances of a fully assembled 2SB mixer using the SIS junction properties. As result, the IRR of our mixer was found to be limited by the RF imbalance, which is caused by complex standing waves created by reflections from the SIS junctions, the RF hybrid and the RF absorption load.**

***Index Terms*—Image rejection ratio (IRR), propagation losses, sideband separating (2SB) mixers, submillimeter wave technology, superconductor–insulator–superconductor (SIS) mixers, superconductor–insulator–superconductor (SIS) tunnel junction, terahertz receivers.**

I. Introduction

ASTRONOMICAL observations for high frequencies such as the Atacama large millimeter array (ALMA) band 9 (602–720 GHz) are restricted by atmospheric conditions. Because of that, for spectral line sources, the sideband-separating (2SB) receiver can provide a better sensitivity than the double-sideband (DSB) one by reducing the atmospheric noise contribution. The actual gain in sensitivity of a 2SB receiver compared to a DSB receiver is a nonlinear function of atmospheric transparency and the receiver parameters, and it should be explicitly addressed.

Manuscript received August 15, 2016; revised October 20, 2016; accepted November 14, 2016. Date of publication December 28, 2016; date of current version January 12, 2017. This work was supported in part by the Dutch Research School for Astronomy (NOVA) under a NOVA-IV ALMA R&D grant, in part by the AETHER of RadioNet under FP7, and in part by the Comisión Nacional de Investigación Científica y Tecnológica under fund CATA-Basal PFB06.

A. Khudchenko, R. Hesper, and J. Barkhof are with the Kapteyn Astronomical Institute, University of Groningen, Groningen 9747 AD, The Netherlands (e-mail: A.Khudchenko@sron.nl; r.hesper@sron.nl; j.barkhof@sron.nl).

A. M. Baryshev is with the Kapteyn Astronomical Institute, University of Groningen, Groningen 9747 AD, The Netherlands, and also with The Netherlands Institute for Space Research, Groningen 9747 AD, The Netherlands (e-mail: a.m.baryshev@sron.nl).

F. P. Mena is with the Electrical Engineering Department, Universidad de Chile, Santiago 8320000, Chile (e-mail: fpmena@u.uchile.cl).

Color versions of one or more of the figures in this paper are available online at http://ieeexplore.ieee.org.

Digital Object Identifier 10.1109/TTHZ.2016.2633528

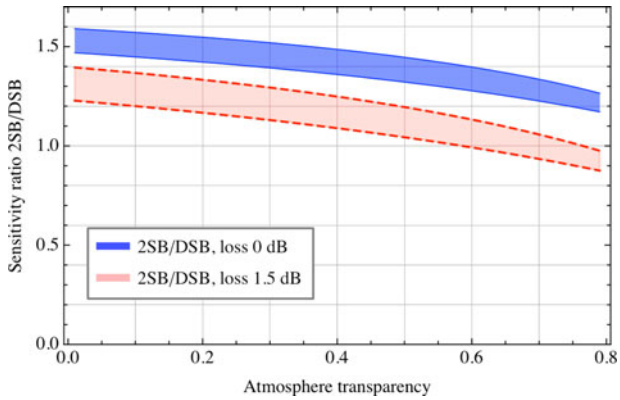

Fig. 1. 2SB/DSB sensitivity ratio vs atmosphere transparency: darker area with solid line borders corresponds to perfect case, then 2SB receiver has no any additional insertion RF losses compare to DSB one, the lighter area with dashed line borders – 1.5 dB of RF insertion loss. The bands represent the spread in noise temperature of the produced band 9 mixers.

From the historical weather conditions at the ALMA location [1], the zenith atmospheric transmission for band 9 can be estimated between 0.1 and 0.6. This is mainly determined by the precipitable water vapor column, and corresponds to an interval from about 2 to 0.3 mm. The upper limit of transmission corresponds to a realistic estimation of good weather conditions, while the bottom one represents the limit at which the atmosphere becomes too opaque for reasonable observations in band 9.

The ratio of the 2SB and DSB sensitivities should be determined independently for the two main observational regimes in radio astronomy: 1) interferometry, where signals of paired antennas are combined in a correlator and 2) single-dish mode (or total power mode in a telescope array, where signals of all the antennas are added up). In addition, two different types of sources should be distinguished: 1) spectral line sources, where the signal is a single narrow spectral line or many narrow lines present in either one or both sidebands and 2) continuum sources, where the signal has a wide spectrum and covers entirely both upper (USB) and lower sidebands (LSB). The 2SB/DSB sensitivity ratio for spectral line sources is the same for both the interferometer and the single-dish mode. Fig. 1 shows the sensitivity ratio, calculated in the same way as in [2], as function of atmospheric transparency for two different values of the internal mixer loss (which will be discussed later). The interferometry mode with continuum sources will reduce the ratios with a factor 1.4 ($\sqrt{2}$). And finally, the total power mode for continuum sources will give a factor of 2 reduction.

The results are calculated for ALMA band 9, taking an atmospheric temperature of 270 K, the mixer single sideband noise temperature as varying from 140 to 250 K (from [3]). The results agree well with estimates in [4]. Additionally, the option of RF insertion loss of 1.5 dB is considered. It can be concluded from Fig. 1 that, in the ideal case, the 2SB/DSB sensitivity ratio can be up to 1.4 on average for spectral line sources, giving an observation time reduction factor of about 2, and without strong changes for continuum sources observations. Potentially, it makes the 2SB band 9 receiver a promising option for future ALMA upgrades, as well as deployment in other observatories. One of the key challenges, apart from optimizing the image rejection ratio (IRR), which is the subject of the current paper, is to reduce the internal losses so far that this ideal case can be approached. The resolution of the latter issue, combined with the insights of this paper, has been subject of continuing research [5].

II. Details of Modular Design

Any millimeter or submillimeter superconductor–insulator–superconductor (SIS) receiver is a complex device consisting of several critical components. As result, it can be favorable to build it out of several blocks tested independently [6], [7], i.e., in a modular way. On the other hand, integrating the parts as much as possible has also benefits, especially for compactness, low losses, and the possibility to integrate intermediate frequency (IF) handling [8]–[10], while facing additional risks of complexity and loosing possibility of testing and replacing individual elements. Anyway, for any particular 2SB receiver, the optimal balance of integration should be found.

Several years ago, a 2SB mixer was developed to investigate the possibility of providing 2SB technology for ALMA band 9 [8]. It was a monolithic split block design with a very high level of integration. The RF hybrid, local oscillator (LO) couplers, LO horn, matched loads, SIS junctions, magnet coils, and magnet conductors for Josephson suppression and dc bias tees were integrated in a single block. Because of the high complexity of the mixer block, involving machining on vastly different scales, it turned out to be very difficult to obtain blocks of required quality. Another disadvantage of the monolithic design was inability to pretest SIS mixer devices separately and replace them individually, facilitating the matching of mixers gains in order to reach a high sideband rejection ratio. As result, an important lesson learned from the monolithic mixer block is the importance of a modular design.

A. Design of RF Block

The modular RF block of our 2SB mixer is depicted in Figs. 2 and 3. It has been designed around the SIS junction holders ("backpieces") used in the ALMA band 9 production [3]. The backpieces are compact, reusable, and easy to mount on a standard band 9 horn for testing and matching. Moreover, since the junctions are in the same RF environment as the single-ended mixers, the previously developed mixer devices can be used.

The magnetic field for Josephson suppression is provided by a superconducting coil in the mixer sidepiece and directed to the junction by Vacoflux magnet conductors, built up from several pieces. The inner pole pieces are inside the hybrid-mixer interface ring, and at the same time provide the angular alignment of the backpiece. The magnetic cross talk between the Josephson suppression coils is about 4%, which is an acceptable level. The thermal cross talk between the deflux heaters is small enough to allow defluxing one mixer without the other one going out of superconductivity.

The RF horn alignment to the hybrid block is done with a precision of 5 μm by visual control using a microscope. It is enough to have negligibly low reflection, which was confirmed later by reproducibility of receiver sensitivity after multiple reassembles.

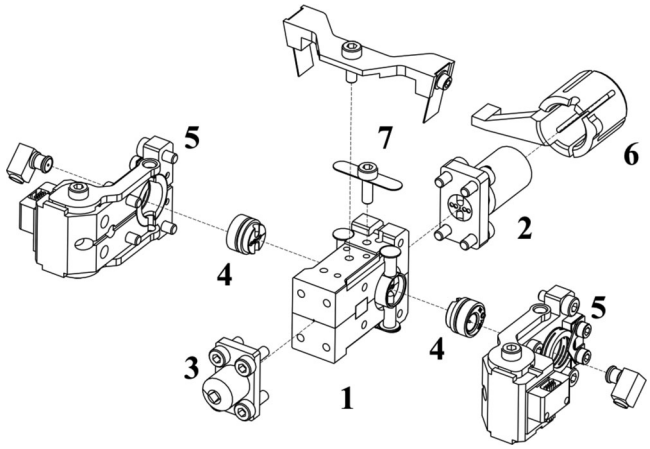

Fig. 2. Exploded view of the modular 2SB mixer block. The major parts are: "1"—a central split block (hybrid block) containing the RF waveguide structure including the loads; "2"—a corrugated RF input horn; "3"—a diagonal LO horn; "4"—two backpieces, holding one SIS device each; "5"—two side-pieces, each containing a magnet coil, most of the magnetic field conductors, heater contact, thermometer, a small PCB with a nano-D connector to export all signals and spring-loaded retainer caps to clamp the backpieces in place; "6"—a "collet" to clamp the mixer by its horn in the optics assembly; "7"—brackets to secure connectors magnet pins and GPO connectors. Two right angle GPO connectors in right-bottom and left-top corners show the way the IF cables are connected to the mixer block.

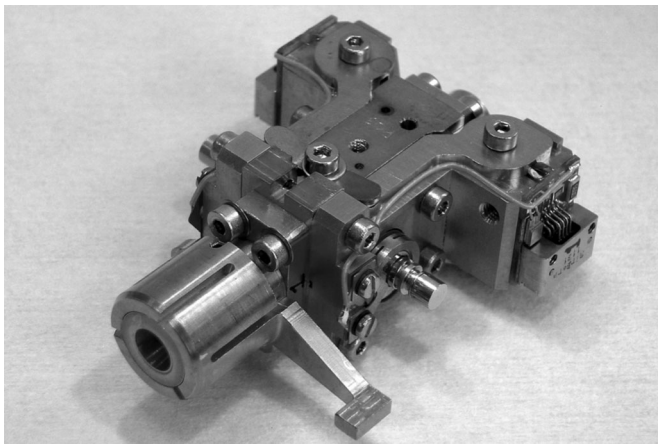

Fig. 3. Photograph of the modular 2SB mixer block. The corrugated RF input horn is on the left, the LO horn is on the back site opposite to it (not visible). One of the standard band 9 mixer back pieces is visible near the center with an installed GPO 50 Ω load to protect the SIS mixer from static discharge.

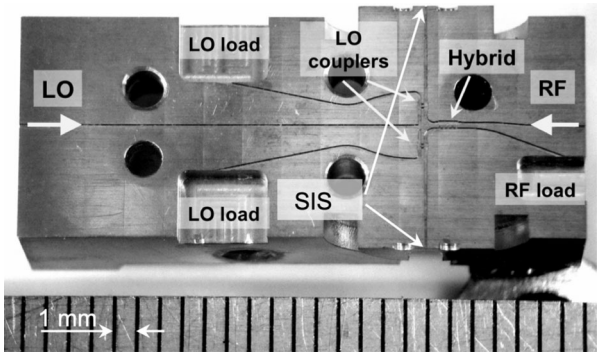

Fig. 4. Photo of the hybrid block showing the RF waveguide structure. Big arrows show path of the LO and RF input signals. The sign "SIS" indicates the location of the SIS junctions after the backpieces are installed.

A more detailed description of the mechanical design together with the modifications of the ALMA band 9 DSB cartridge to 2SB mode and possible options for upgrade can be found in [11].

B. RF Waveguide Structure

The waveguide implementation of the 2SB mixing scheme (shown in Fig. 4) is very similar to the one used before in the monolithic block [8]. The transverse waveguide dimensions are $310 \times 145\,\mu\text{m}^2$. The quadrature hybrid is made as a 5-line branchline coupler, the LO couplers use two branchlines. The LO splitter is a simple impedance-matched E-plane tee. The left-over LO power after the LO couplers is absorbed in two matched LO loads. The energy reflected from the mixers (as long as it is in phase and of the same amplitude) emerges from the hybrid in the waveguide going to an RF load.

The loads are made by running the waveguides at a shallow angle (about 20°) into a relatively large block of absorber material (Eccosorb MF112). The blocks were given narrow cutouts to make them fit tightly against the waveguide orifice by slight elastic deformation.

C. IF Chain

The outputs of the RF block deliver the 4–12 GHz IF signals. They are connected by length-matched semirigid cables to the inputs of a 90° IF hybrid developed by Centro Astronómico Yebes [12]. The IF hybrid has an amplitude imbalance less than ± 0.3 dB and phase imbalance not exceeding $\pm 2°$, over the 4–12 GHz band. The further IF chain consists of 4–12 GHz isolators and cryogenic amplifiers developed by Yebes as well [13].

III. Receiver Performance

We fabricated the RF waveguide blocks out of two types of materials: 1) CuTe alloy (type C14500/CuTeP) and 2) bronze, plated electrolytically by a 2 μm thick gold layer without any interface layer in between. This is mentioned specifically because we have observed a large impact of the RF waveguide block material on the receiver performance, as will be discussed below. The other parts of the receivers, including SIS mixers and IF hybrid, were the same for all the measurements presented here.

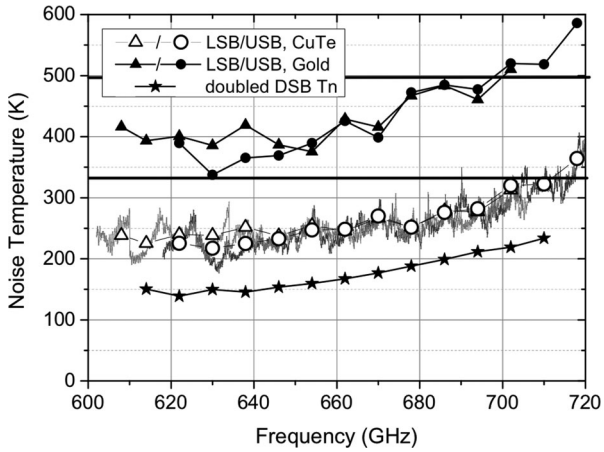

Fig. 5. Comparison of the uncorrected single-sideband T_n for the CuTe hybrid block (empty circles and triangles) and gold-plated block (filled circles and triangles) with the sum of DSB T_n of the single-ended SIS-junctions (stars). Thin gray curves show the distribution of T_n within the IF bands. The ALMA specification is shown by solid horizontal lines, 80% of the band should not exceed 336 K while all points should be below the 500 K level [14].

A. Noise Temperature

The single-sideband noise temperature T_n of the 2SB receivers was measured by the standard Y-factor method using hot (300 K) and cold (77 K) loads. The results for both LSB and USB are presented in Fig. 5. Each point, which is depicted by a circle, triangle, or star corresponds to an average of T_n over the IF band of 8 GHz for various LO frequencies. In contrast, the distribution of T_n within the IF is displayed by the thin gray solid curves, which are measured with a frequency resolution of about 50 MHz. The flatness of the fine-resolution curves demonstrates a high quality of the performance over the IF bands.

With the CuTe block, the uncorrected T_n is within an interval of 200–380 K. Since the measured T_n is below 336 K in 95% of the 600–720 GHz band, it is well within the ALMA specification [14]. The gold-plated RF waveguide block has much higher T_n. To estimate the increase of T_n due to the RF waveguide structure, the doubled DSB T_n measured individually for the used SIS mixers is also plotted in Fig. 5 (filled stars). It indicates the T_n level expectation corresponding to a perfect lossless RF waveguide structure.

One can see from the measurements that the increase of T_n is about 40% for the CuTe block and 120% for the electrolytically gold-plated block. Since the physical temperature of all the RF parts is 4 K, the T_n increment is caused by loss of the RF signal, giving 1.5 and 3.5 dB loss for CuTe and gold, respectively. It should be mentioned here that for the DSB measurements, a 5% beam splitter at 4 K level was used, giving 0.2 dB signal loss, while the 2SB block has 12% LO coupler giving 0.5 dB loss of signal. Nevertheless, this would yield only 0.3 dB difference and does not explain the rest. In total, this amounts to 1.2 and 3.2 dB losses for CuTe and gold-plated blocks, respectively. The level of the losses is flat over the total frequency band, which points to a resistive nature.

To investigate the reason of the RF losses, we have fabricated test-blocks with straight waveguides of dimensions $a =$

310 μm, $b = 145$ μm (the same as in the RF block) and a length of 12 mm, which is about equal to the length of the waveguide between the RF horn interface and the SIS junctions (see Fig. 4). The test-blocks have been fabricated also by micromilling out of different materials such as CuTe, oxygen-free Cu (type C10200, 99.95% purity), and bronze. Later on, some blocks were gold-plated. In the measurement, a test-block has temperature of 4 K. It is placed between the horn and the DSB SIS mixer, which causes a reduction of the sensitivity when compared to the system without the block. The factor of the T_n increase yields the level of the losses. The detailed analysis of the results will not be presented here, but from the measurements, we conclude that the lowest loss level was found to be as low as 0.6–0.7 dB (50–60 dB/m) for both CuTe alloy and oxygen-free Cu. For the electrolytically gold-plated test-blocks, the losses were about 1.5 dB (125 dB/m).

A theoretical estimate of the waveguide loss can be made by using a standard approach described in [15], when electrons in a skin depth layer determine the conduction process. Such an approach gives the loss level of 75.8 dB/m at 650 GHz in a rectangular waveguide of 310 $\times$ 145 μm^2 made from Cu with conductivity of 5.85 $\times$ 10^7 S/m, at a temperature of 300 K. The losses are expected to go down when cooling the metal. However, the so-called anomalous skin effect starts playing a role in metals at low temperatures for high-frequency signals [16], [17]. This effect takes place when the electron mean free path becomes large compared to the classical skin depth. For C10100 Cu with RRR = 106 at 650 GHz, the ratio of the mean free path l to the classical skin depth δ is about 515 at 4 K ($\delta_{4\,\mathrm{K}} = 8.2$ nm, $l_{4\,\mathrm{K}} = 4.1$ μm) and 0.47 ($\delta_{300\,\mathrm{K}} = 84$ nm, $l_{4\,\mathrm{K}} = 39$ nm) at 300 K [16], which means that, at cryogenic temperatures, the material is deep in the anomalous skin effect regime. Actually, Cu is close to the anomalous regime already at room temperature and a slightly higher loss than the one calculated above is expected. Calculation of the loss by using the approach of [16] and [17] gives 59 dB/m for our waveguide at 650 GHz and 4 K. As result, the loss level for the length of 12 mm is 0.7 dB, which is in a good agreement with the experimental results for the test blocks and indicates the fundamental lower limit for a waveguide of these dimensions, at this temperature, made of copper.

Despite of equal waveguide lengths, the RF waveguide block has 0.5 dB higher resistive losses than the test-block for CuTe and 1.7 dB correspondingly for gold. We suspect the material, fabrication, surface roughness, including the walls roughness, and interface slot issues could be the reason. We expect to have Ra of about 100 nm for CuTe, similar to [18]. In case of electrolytic gold-plating, the roughness should be even higher.

B. IRR

To determine the IRR of the receivers, the standard approach [19] was applied. In this, a small power test signal is injected by a beam splitter into the RF horn, which looks at the hot/cold load, and measured in both LSB and USB IF outputs. The results are presented in Fig. 6 for receivers with both the CuTe and gold-plated waveguide blocks. One can see, the IRR for CuTe is better than 11.5 dB in the entire band, while in case of gold-plating, it exceeds the 15 dB level for 99% points and stays above 20 dB on average. It should be mentioned that the presented measurements are made at fixed bias voltages of the SIS junctions (each at 2 mV) without any optimization by these parameter. Even then, the presented results clearly fit in the ALMA specification of 10 dB [14].

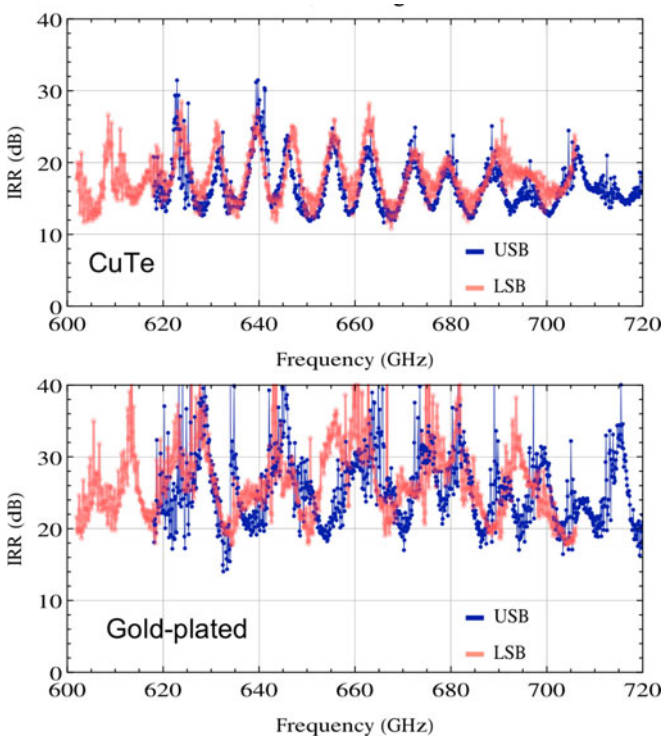

Fig. 6. IRR over the RF band for both upper and lower sidebands. The top graph corresponds to the CuTe RF waveguide block and bottom graph to the gold-plated one. Each curve is stitched of 13 IF bands measured for different LO frequencies, spaced 8 GHz apart, yielding a contiguous RF coverage. The frequency resolution is 50 MHz.

A detailed analysis of the large difference between IRR for waveguide blocks from different material will be given below. Nevertheless, from the current results, an important conclusion can be made: the SIS mixers gain and the IF hybrid have such a small imbalance that an IRR level of 20 dB is attainable, and, in case of the CuTe block, the waveguide block itself is the main source of imbalance, limiting the IRR value.

IV. Characterization Methods

The imbalance of 0.5 dB in the IF hybrid [12] and 1 dB in the RF hybrid [8] leads to an expected IRR better than 22 dB over the entire frequency range. This specific discrepancy, between the expectation and the measurements, encouraged us to investigate the problem in depth. For this, we need tools to do in-situ characterization of the integrated system, because the interactions between the components can create deviations as large as those of the individual components themselves.

A. RF Balance

Looking at the IRR curves on Fig. 6, one can see a quasi-periodic structure, which is especially clear for the CuTe block.

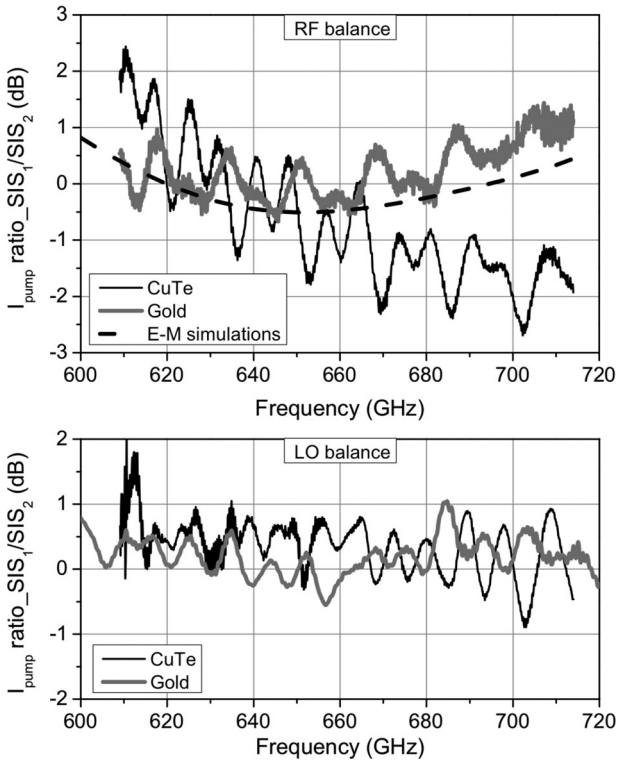

Fig. 7. Pumping balance between the two SIS devices in the mixer block, measured as the ratio of the SIS pumping currents at 2 mV bias voltage while sweeping the test signal (LO signal) frequency. Top graph shows the RF balance, while the bottom one the LO balance: black solid curves are measured for CuTe waveguide block, gray solid curves—for gold-plated one, dashed curve at the top plot shows the result of E-M simulations of the RF hybrid balance corresponding to [8]. Due to a small fabrication error in the hybrid depth, the curve for CuTe RF block on the top plot has a deviation from the E-M simulations. Here, SIS_1 and SIS_2 correspond to the junctions at bottom and top positions, respectively, according to Fig. 4.

The period of the structure is about 8 GHz and it corresponds to the length of 25 mm in our waveguide, which is approximately twice the distance between the RF load and the SIS mixers (see Fig. 4). Such a coincidence could be explained by the presence of standing waves in the waveguide block between the SIS junctions and the RF load, which can create an additional RF imbalance. Furthermore, this hypothesis is strongly supported by the fact that for the gold-plated block with higher waveguide losses, i.e., the smaller the standing waves, the much better the IRR measured.

To study the RF balance of the waveguide hybrid block in the operating regime (at 4 K and with the installed SIS junctions), we have developed a method based on proportionality of the SIS junction photon assistant current at a fixed bias voltage to the RF power reaching the junction [20]. For the first photon step, the dependence of the photon assistant current on the incident RF power is described by a Bessel function, which is linear for low pumping currents (the pumping current level was kept below 20% of the gap current). Basically, the test signal was injected through the RF horn and the SIS pumping currents at 2 mV were measured. The ratio of the pumping currents gives exactly the power balance of the receiver RF signal path. Results of the measurements are presented in the top graph of Fig. 7 (the bottom graph shows the LO balance and will be discussed later).

The RF balance measurements have clear periodic pattern fully confirming the idea of strong parasitic reflections. There are two clearly distinguishable waves on the curves with periods of about 8.2 GHz and close to 17 GHz at frequency around 650 GHz, which gives waveguide lengths of 24 and 11.7 mm, respectively. These numbers are very close to the doubled distances SIS – RF load and SIS – RF hybrid, respectively (see Fig. 4).

From the symmetry point of view, not every reflection in the waveguide block should contribute to imbalance. For example, standing wave between the SIS mixers and the LO couplers on each sight will give equivalent contribution to each mixer without influencing the total balance. The origin of the "standing" wave on Fig. 7 is based on asymmetry induced by the RF hybrid. Let us consider the mechanism in detail. The RF signal is split in the hybrid on two parts, the first half goes to the first SIS mixer (top one on Fig. 4) and other half goes to the second SIS (bottom one on Fig. 4) with a $\pi/2$ phase delay. The SIS junctions are known to reflect a significant part of the power, up to –10 dB or even more [21]. For simplification, let us assume that the amplitudes of the reflected signals are the same. Because of the $\pi/2$ phase delay in the RF hybrid, all the power of the reflected signals ends up only in the branch of the RF load. The reflection from the RF load is split in the RF hybrid and every part combines with the main RF signal. For the top branch, the reflection component has an additional phase shift of $\pi + 2\pi l/\lambda$ relative to the main RF signal (the reflection crossed the RF hybrid twice, giving in total phase delay of π). Meanwhile, for the bottom branch such a difference is only $2\pi l/\lambda$ (both the main signal and the reflection cross the hybrid one time). Finally, this means that the RF load reflection contributes in contra-phase to the SIS mixers, i.e., directly gives the RF imbalance. This mechanism explains the 8.2 GHz wave on the balance curves. The 17 GHz period wave can be described in a similar way. The only difference is that the signals reflected from the SIS junctions go through the RF hybrid in reverse direction (for example, from the top SIS junction to the bottom one directly through the hybrid). The amplitude of the described imbalance is determined by the RF hybrid isolation, which determines, for instance, the leakage from the RF input port to the RF load, and it is normally very close to the S_{11} parameter.

The described imbalances are interfering with each other resulting in the final balance and the IRR patterns. Comparing results for CuTe and gold-plated blocks on Fig. 7, one can say that the peak-to-peak amplitudes are about two times different. It means that the reflected signals, which induce these imbalances, have roughly two times different amplitudes (6 dB difference in power). This observation agrees well with the IRR measurements, where the difference in IRR at the bottom level of the curves is on average exactly 6 dB (12 and 18 dB for CuTe and gold-plated blocks, respectively, see Fig. 6). The losses estimated from the T_n measurements are also in good qualitative agreement with these results, while quantitatively—not fully. In particular, for the 8.2 GHz wave with traveling distance of 24 mm, the difference in losses between the blocks is (3.5 – 1.5 dB) $\times$ 2 = 4 dB, and about twice less for the 17 GHz wave. It gives only 60% and 25% difference for amplitudes of imbalances, which is certainly less than estimated from the balance measurement. This discrepancy should be investigated.

B. LO Balance

The LO balance is also important for the 2SB receiver performance. Basically, the LO amplitude imbalance will vary pumping levels of the SIS junctions leading to change of the mixer gains. At the same time, the presence of phase imbalance of LO signals will directly reduce the IRR.

For characterization of the LO balance, we have used a similar approach as for the RF. The LO signal was swept through the entire frequency band, while the SIS pumping currents were measured. The result for the CuTe block is presented in the bottom panel of Fig. 7.

Due to symmetry (see Fig. 4), the LO paths for both SIS junctions are equal and any reflections from LO loads or LO couplers are contributing to the junction pumping in the same way, i.e., not leading to any imbalance. The only intrinsic asymmetry of the current waveguide design is in the hybrid. Therefore, it can influence the LO balance, because both LO signals reflected from SIS junctions can go to the RF load (being split in power by two in the hybrid) and can be partially reflected back. At that, one of them is passing through the hybrid twice and turns its phase by π relative to the other one. As result, these reflections contribute directly to the LO imbalance. The described mechanism is almost the same as for the 8.2 GHz wave in the RF balance and should lead to the same period that is fully confirmed by the measurements shown in Fig. 7.

An important difference is that the 17 GHz wave is not present in the LO imbalance. Here, in contrast to the RF case, the phase of the signals reflected from the SIS junctions and going through the hybrid isolation path is the same relative to the LO port.

Finally, we come to a conclusion: the LO balance is mainly disturbed by reflections from the SIS junctions and the RF load.

C. IF Balance

According to the manufacturer, the IF hybrid has an amplitude imbalance less than ± 0.3 dB over the 4–12 GHz band [12]. However, the total IF balance of the 2SB receiver also can be different due to reflections. To estimate it, we have developed a special method. Since the level of shot noise generated by an SIS junction above the gap voltage is well known [22], one can use both SIS mixers as controlled IF white noise sources for IF balance calibration (similar to calibration of IF amplifiers). We biased the junctions to 5 and 8 mV and measured the IF output spectra for three (out of four) bias combinations: 5 and 5 mV; 5 and 8 mV; 8 and 5 mV. For the first bias combination (5 and 5 mV), the measured USB output IF spectrum $P_{\mathrm{USB\_5-5}}$ can be presented as

$$P_{\mathrm{USB\_5-5}} = (P_1 G_{1-\mathrm{USB}} + P_2 G_{2-\mathrm{USB}})\, G_{\mathrm{IF\_USB}}$$

where $G_{1-\mathrm{USB}}$ is the power gain between mixer SIS_1 (see diagram in Fig. 8) and the USB output of the hybrid, and $G_{2-\mathrm{USB}}$ is the power gain between mixer SIS_2 and the USB output; P_1 and P_2 are the powers of SIS_1 and SIS_2 shot noise at bias of 5 mV; $G_{\mathrm{IF\_USB}}$ is the gain of the USB IF chain after the hybrid; P_N is the noise power generated by the USB IF amplifiers.

Taking *K* as the ratio of shot noise power between 5 and 8 mV, similar equations can be written for the bias combinations 5 and 8 mV, and 8 and 5 mV,

$$P_{\mathrm{USB\_5-8}} = (P_1 G_{1-\mathrm{USB}} + K P_2 G_{2-\mathrm{USB}} + P_N)\, G_{\mathrm{IF\_USB}},$$
$$P_{\mathrm{USB\_8-5}} = (K P_1 G_{1-\mathrm{USB}} + P_2 G_{2-\mathrm{USB}} + P_N)\, G_{\mathrm{IF\_USB}}.$$

By preselecting the SIS junctions with similar *IV*-curves, we can make $P_1 = P_2$. Under this condition, the following ratio can be derived:

$$\frac{G_{1-\mathrm{USB}}}{G_{2-\mathrm{USB}}} = \frac{P_{\mathrm{USB\_8-5}} - P_{\mathrm{USB\_5-5}}}{P_{\mathrm{USB\_5-8}} - P_{\mathrm{USB\_5-5}}}$$

which is the ratio of the power gains of the 90° branch (diagonal) and the 0° one (straight) for the USB output. Equations for the LSB IF port are very similar. Both USB and LSB ratios determined experimentally are presented in the top panel of Fig. 9.

The curves in Fig. 9 show a much worse performance than the IF hybrid gain imbalance determined by the manufacturer

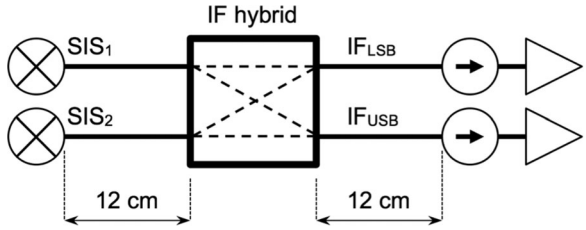

Fig. 8. Block diagram showing IF chain including the IF hybrid, the SIS mixers, isolators, IF amplifiers, and the connecting cables.

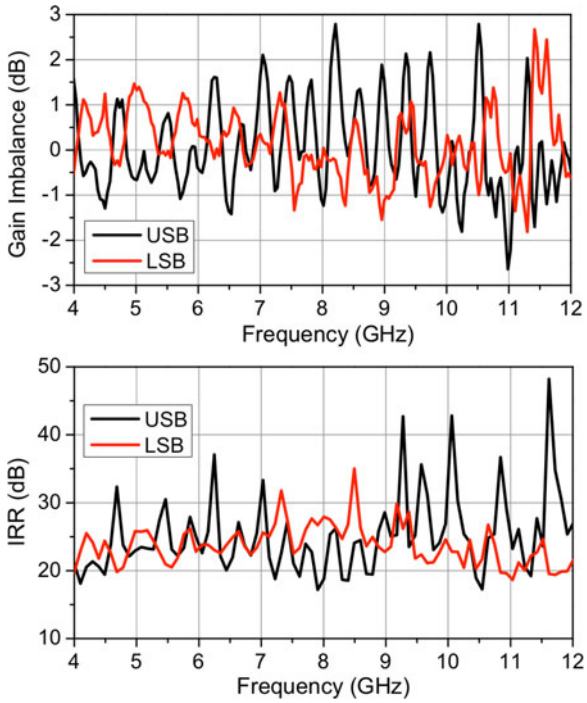

Fig. 9. Top panel shows the ratio of the diagonal and the straight power gains between the SIS mixers and the IF output versus intermediate frequency: USB—black line, LSB—gray line. Bottom panel shows the IRR versus the intermediate frequency for LO frequency of 614 GHz (corresponds to the bottom panel of Fig. 6). The curves presented on both graphs were obtained for the gold-plated waveguide block.

[12] (3 dB instead of 0.3 dB). Here, we have again a periodic pattern, which is not presented in the measurements made by the manufacturer for the single IF hybrid, but it can strongly influence the balance. Notably, by looking on the IRR curves with high-frequency resolution in IF representation (see bottom graph in Fig. 9), one can find a similar periodic structure showing the importance of this issue for the receiver's performance.

The period of the wave in the balance curve is about 400 MHz corresponding to an electric distance of 50 cm in SMA cables with teflon filling. The SIS junctions are connected to the IF hybrid by 12-cm cables, and the cables of about the same length are used between the hybrid and the isolators. Therefore, the periodic pattern could be caused by reflection from the isolators, hybrid, and SIS mixers interacting through the hybrid. However, the effect of the estimated IF amplitude imbalance seems to be exaggerated by the fact that at the used bias points (5 and 8 mV) the output impedances of the SIS devices deviate few times from their operational design values. In real operation, the mismatches are likely to be much smaller, giving less reflection from the SIS junctions and, as result, lower imbalance.

In summary, the presented method can be useful to estimate the IF chain imbalance and can be used as a tool to compare different hybrids and different IF chains in operating receivers. It can be set as a standard "health check" test for any 2SB receiver.

V. Conclusion

We have completed a modular 2SB receiver for 600–720 GHz showing both the IRR and the noise temperature well within typical specifications for current observatories.

The waveguide losses due to the anomalous skin effect were found to be an important issue for the receiver performance at high frequencies. Moreover, it was shown that the IRR is strongly influenced by reflections in both IF and RF parts of the mixer. The main imbalance in the RF part is due to reflections from the SIS mixers and the RF load. Additionally, the RF hybrid isolation should be minimized. The characterization methods developed here help to check the actual IF and RF imbalances for an assembled and operating receiver. The methods can be applied to any SIS 2SB receiver.

Acknowledgment

The authors would like to acknowledge J. Pizarro, Universidad de Chile, for machining the hybrid block. The envelope of the mixer block and the associated components were originally designed by G. Gerlofsma. The waveguide design of the original hybrid block was due to J. Kooi. The authors would also like to recognize the efforts of the group led by T. M. Klapwijk producing the mixer devices during the ALMA band 9 production. Finally, the authors thank J. Adema and A. Koops for their organizational and management support.

References

[1] A. Otarola, M. Holdaway, L.-E. Nyman, S. J. E. Radford, and B. J. Butler, "Atmospheric transparency at chajnantor: 1973–2003," Nat. Radio Astron. Observ., Socorro, NM, USA, ALMA Memo 512, 2005.

[2] A. Khudchenko *et al.*, "Sideband separating mixer for 600–720 GHz for ALMA band 9 upgrade," *Proc. SPIE*, vol. 8452, 2012, Art. no. 845214.

[3] A. M. Baryshev *et al.*, "The ALMA band 9 receiver. Design, construction, characterization, and first light," *Astron. Astrophys.*, vol. 577, p. A129, 2015.

[4] A. R. Thompson and L. R. D'Addario, "Relative sensitivity of double- and single-sideband systems for both total power and interferometry," Nat. Radio Astron. Observ., Socorro, NM, USA, ALMA Memo 304, 2000.

[5] R. Hesper, A. Khudchenko, A. M. Baryshev, J. Barkhof, and P. Mena, "A new high-performance sideband-separating mixer for 650 GHz," *Proc. SPIE*, vol. 9914, 2016, Art. no. 99140G.

[6] B. Billade *et al.*, "Performance of the first ALMA band 5 production cartridge," *IEEE Trans. Terahertz Sci. Technol.*, vol. 2, no. 2, pp. 208–214, Mar. 2012.

[7] D. Maier, J. Reverdy, D. Billon-Pierron, and A. Barbier, "Upgrade of EMIR's band 3 and band 4 mixers for the IRAM 30 m telescope," *IEEE Trans. Terahertz Sci. Technol.*, vol. 2, no. 2, pp. 215–221, Mar. 2012.

[8] F. P. Mena *et al.*, "A sideband-separating heterodyne receiver for the 600–720 GHz band," *IEEE Trans. Microw. Theory Techn.*, vol. 59, no. 1. pp. 166–177, Jan. 2011.

[9] A. R. Kerr, S.-K. Pan, S. M. X. Claude, P. Dindo, A. W. Lichtenberger, and E. F. Lauria, "Development of the ALMA-North America sideband-separating SIS mixers," in *IEEE MTT-S Int. Microw. Symp. Dig.*, 2013, pp. 1–4.

[10] D. Maier, J. Reverdy, L. Coutanson, D. Billon-Pierron, C. Boucher, and A. Barbier, "Fully integrated sideband-separating mixers for the NOEMA receivers," in *Proc. 25th Int. Symp. Space Terahertz Technol.*, 2014, pp. 80–84.

[11] R. Hesper, G. Gerlofsma, F. P. Mena, M. Spaans, and A. M. Baryshev, "Construction of a side band separating heterodyne mixer for band 9 of ALMA," in *Proc. 18th Int. Symp. Space Terahertz Technol.*, 2007, pp. 39–43.

[12] I. Malo, J. D. Gallego, C. Diez, I. López-Fernández, and C. Briso, "Improved multi-octave 3 dB IF hybrid for radio astronomy cryogenic receivers," in *Proc. 20th Int. Symp. Space Terahertz Technol.*, 2009, pp. 300–306.

[13] I. López-Fernández, J. D. Gallego, C. Diez, and A. Barcia, "Development of cryogenic IF low noise 4–12 GHz amplifiers for ALMA radio astronomy receivers," in *IEEE MTT-S Int. Microw. Symp. Dig.*, 2006, pp. 1907–1910.

[14] W. Wild and J. Payne, "Specifications for the ALMA front end assembly," 2000.

[15] E. Maxwell, "Conductivity of metallic surfaces at microwave frequencies," *J. Appl. Phys.*, vol. 18, no. 7, pp. 629–638, 1947.

[16] R. Finger and A. R. Kerr, "Microwave loss reduction in cryogenically cooled conductors," *Int. J. Infrared Millim. Waves*, vol. 29, no. 10, pp. 924–932, 2008.

[17] A. B. Pippard, "Metallic conduction at high frequencies and low temperatures," *Adv. Electron. Electron Phys.*, vol. 6, pp. 1–45, 1954.

[18] C. E. Groppy, B. Love, M. Underhill, and C. Walker, "Automated CNC micromachining for integrated THz waveguide circuits," in *Proc. 21th Int. Symp. Space Terahertz Technol.*, 2010, pp. 338–341.

[19] A. R. Kerr, S. K. Pan, and J. E. Effland, "Sideband calibration of millimeter-wave receivers," Nat. Radio Astron. Observ., Charlottesville, VA, USA, ALMA Memo 357, 2001.

[20] J. R. Tucker and M. J. Feldman, "Quantum detection at millimeter wavelength," *Rev. Mod. Phys.*, vol. 57, no. 4, pp. 1055–1113, 1985.

[21] Y. Uzawa *et al.*, "A sensitive ALMA band 10 SIS receiver engineering model," *Supercond. Sci. Technol.*, vol. 22, no. 11, 2009, Art. no. 114002.

[22] K. K. Likharev, *Dynamics of Josephson Junctions and Circuits*. London, U.K.: Gordon and Breach, 1984.

Andrey Khudchenko received the M.S. degree in applied physics and mathematics and Ph.D. degree in radiophysics from the Moscow Institute of Physics and Technology, Moscow, Russia, in 2007 and 2009, respectively.

From 2004 to 2008, he was an Engineer and, in 2009, a Researcher with the Kotel'nikov Institute of Radio Engineering and Electronics, Russian Academy of Sciences, Moscow. Since 2009, he has been an Instrument Scientist with The Netherlands Institute for Space Research SRON, Utrecht, The Netherlands, working on the development of new heterodyne THz instruments. It includes development of sideband-separating receiver for the ALMA band 9, CHAMP+ high mixers for the APEX telescope, and work on stabilization of quantum cascade lasers for hot electron bolometer receivers.

Ronald Hesper received the M.Sc. degree in experimental solid state physics from the University of Leiden, Leiden, The Netherlands, and the Ph.D. in experimental solid state physics from the University of Groningen, Groningen, Netherlands.

Since 2000, he has been an Instrument Scientist with the Kapteyn Astronomical Institute, University of Groningen. From 2000 to 2008, he was involved with the technical and technological development of the ALMA band 9 receivers, including the process of industrialization; from 2008 to 2013, on the development of a sideband-separating mixer upgrade for the ALMA band 9 receivers; and from 2013 to the beginning of 2015, on the industrialization of the ALMA band 5 receivers. Currently, he is involved in the development of new (arrayable) heterodyne detector technologies at frequencies around 1 THz.

Andrey M. Baryshev received the Master's degree (*summa cum laude*) in physical quantum electronics from the Moscow Institute of Physics and Technology, Moscow, Russia, in 1993, and the Ph.D. degree from the Technical University of Delft, Delft, The Netherlands, in 2005.

He is currently a Senior Instrument Scientist. Since 1998, he has been with the SRON Low Energy Astrophysics Division and the Kapteyn Astronomical Institute, University of Groningen, Groningen, The Netherlands. Since 2000, he has been involved in a joint effort to develop an SIS receiver (600–720 GHz) for the ALMA. In 2013, he became an Associate Professor of astronomical instrumentation for the far-infrared with the Kapteyn Astronomical Institute, University of Groningen. His main research interests include the areas of heterodyne and direct detectors for large focal plane arrays at THz frequencies, and quasi-optical system design and experimental verification.

Dr. Baryshev was the recipient of a Netherlands Organisation for Scientific Research-VENI grant for research on heterodyne focal plane array technology in 2008, and an EU commission Starting Researcher Grant for work on direct detector focal plane arrays in 2009.

Jan Barkhof received the M.Sc. degree in applied physics from the University of Groningen, Groningen, The Netherlands.

From 1999 to 2004, he was an Optical Researcher with Pfizer, where he was involved with an accommodating intra-ocular lens. Since 2004, he has been a Test Engineer with the Kapteyn Astronomical Institute, University of Groningen, developing test systems and software for verifying the quality of ALMA band 9 and band 5 receivers.

Fausto Patricio Mena received the B.S. degree in physics from the Escuela Politécnica Nacional, Quito, Ecuador, in 1994, and the M.S. and Ph.D. degrees from the University of Groningen, Groningen, The Netherlands, in 2000 and 2004, respectively, both in physics.

In 2004, he joined the Low Energy Division, Netherlands Institute for Space Research (SRON), as an Instrument Scientist. Since 2008, he has been a Professor with the Electrical Engineering Department, Universidad de Chile, Santiago, Chile, where he leads the Millimeter and Submillimeter Wave Laboratory.